

Disorder-Induced Time-Dependent Diffusion in Zeolites

Ligang Chen, Marco Falcioni, and Michael W. Deem

Department of Chemical Engineering

University of California

Los Angeles, CA 90095-1592

August 10, 2018

Abstract

We suggest that disordered framework aluminums and non-framework cations can create a disordered electrostatic potential in zeolites that can lead to a discrepancy between diffusivities measured by microscopic and macroscopic experimental techniques. We calculate the value of the discrepancy and the characteristic time scale at which it occurs for several ionic and polarizable species diffusing in zeolites. For ionic species, a discrepancy is almost inevitable. For polarizable species, a significant discrepancy may occur in some zeolites only for long alkanes or large species such as benzene.

1 Introduction

Disordered microporous materials, such as zeolites, microporous carbons, pillared clays, and superionic conductors, have a wide range of applications in fields such as catalysis,

separation, remediation, and sensing. In all of these uses, the dynamical behavior of the sorbed molecules or ions can be a constraining factor. Due to the complicated guest-host interactions in these systems, our ability to predict the dynamical behavior on all time scales is still limited. Accurate prediction of diffusivities is, however, an important component in the design of practical processes using microporous materials.

Among these materials, zeolites have been the focus of particularly intense research efforts due to their wide industrial use and unique crystal structures. Significant effort has been devoted to understanding diffusion in particular.¹ Despite this study, a fundamental question persists for some classes of zeolites: What causes the well-known discrepancy between the diffusivities measured with macroscopic and microscopic techniques? Macroscopic methods, such as the zero-length column (ZLC) technique² and the Wicke-Kallenbach (WK) membrane method,³ typically measure transport diffusivities under a concentration gradient. The time scales involved in the macroscopic experiments are long ($\simeq 1$ s). Microscopic techniques, such as NMR, measure self-diffusivities by following the motion of tagged molecules. In this case the system is kept under equilibrium conditions. The NMR technique samples motion on the Ångstrom length scale and probes relatively short time scales ($\simeq 10^{-12}$ – 10^{-8} s) for the diffusivities typical in zeolites. Mesoscopic methods, such as NMR pulsed field gradient (PFG)⁴ and quasi-elastic neutron scattering (QENS),⁵ also follow the microscopic motion of diffusing species. These methods are time-scale limited, able to access the 10^{-11} – 10^{-3} s range. The diffusivities measured using macroscopic techniques can disagree from those measured by microscopic techniques by one or more orders of magnitude. For example, the diffusivity of benzene in NaX crystals at 403K is found to be $1 \times 10^{-10} \text{ m}^2\text{s}^{-1}$ by NMR, but $4.5 \times 10^{-12} \text{ m}^2\text{s}^{-1}$ by ZLC.⁶

Several explanations for the discrepancy between macroscopic and microscopic diffusivities have been offered, including an extracrystalline resistance, surface barriers to mass transfer, and internal heat conduction effects.¹ To date, however, there is no general theory that can satisfactorily explain the discrepancy. Recent computer simulations have begun to shed light on the understanding of this long-standing puzzle. It appears that different types of molecular motions happen at different time scales. Molecular dynamics simulations by Maginn *et al.*, for example, reveal that the time constant associated with molecular rearrangements of alkanes may be greater than the time constant for motion along a given channel.⁷ Similarly, kinetic Monte Carlo simulation studies of benzene in zeolites by Auerbach *et al.* suggest that, due to the different experimental time scales, PFG NMR measures the intercage diffusivity, while the NMR relaxation method measures the intracage diffusivity.⁸

What these simulation studies suggest, and indeed what the discrepancy between microscopic and macroscopic diffusivities suggests, is that the diffusivity is actually time dependent. That is, for some sorbates in some zeolites, there seems to be one value of the diffusivity, D_0 , associated with motion on the Ångstrom scale and another, smaller, value, D_∞ , associated with motions on longer spatial scales. Such a time-dependent diffusivity can arise from an unusual time dependence of the mean-square displacement of the diffusing species. In this paper, we provide a theory to calculate the diffusivity on different time and length scales. This theory gives not only the ratio D_∞/D_0 , but also the characteristic time and length scale on which the measured diffusivity changes most dramatically.

Although not generally appreciated, disorder within the zeolite framework can have a dramatic effect on the measured diffusivity. The aluminum framework species as well as the associated, non-framework cations create a disordered electrostatic environment for diffusing

species if the aluminums or cations are randomly sited. The strength of the randomness is determined by the aluminum loading, which can vary from a 1:1 Si:Al ratio to a 3000:1 or higher Si:Al ratio. Higher levels of aluminum loading require higher densities of exchangeable cations.⁹ Together, the framework aluminum and non-framework cations create a random environment and lead to a lower ratio of D_∞/D_0 .¹⁰ On the other hand, the disorder can either increase or decrease the microscopic diffusivity D_0 . In the absence of any specific interactions between the diffusing species and the disordered ions, one would expect D_0 to decrease with increasing disorder. For chemisorption-type interactions typical of nucleophilic species, D_0 may increase with an increasing density of cationic sites since the hopping distance between the sites decreases, yet the binding energy per site may remain constant.¹¹

In this paper, we model the long-distance features of the random electrostatic potential in the zeolite with a particularly simple, Gaussian form. We analyze this model to give an explicit form of the time-dependent, experimental diffusivity $D(t)/D_0$. With this result we can predict both the ratio of the macroscopic to the microscopic diffusivity and the time or length scale at which the difference between the two values becomes apparent. If this time scale is greater than that accessed by, say, the NMR technique, then disorder provides one possible mechanism for a discrepancy between microscopic and macroscopic diffusion measurements.

To perform this analysis, we use a field theoretic formulation of the diffusion process. While the theoretical treatment is involved, the physical mechanism considered is simply the slowing down of a diffusing species by the random electric fields within the zeolite. Our paper is organized as follows. In Section 2 we use renormalization group theory to derive the time-dependent diffusivity in terms of the disordered environment within the zeolite. The

long-time renormalization group result is matched to a short-time perturbation theory to give an explicit prediction for the diffusivity. In Section 3 we describe Monte Carlo simulations that validate the time-dependent theory. Several forms of random disorder are studied, and some numerical issues are discussed. In Section 4 we apply the theory to zeolites. The reader interested primarily in how disorder may explain the discrepancy between microscopic and macroscopic measurements of the diffusivity may wish to skip directly to this section. Diffusion of both ionic and polarizable species is considered in this section. Values of the discrepancy between microscopic and macroscopic measurements are predicted in several cases, and the characteristic time and length scales when the discrepancy becomes apparent are also given. For measurements of ionic diffusivities, discrepancies are almost inevitable. For polarizable species, discrepancies can be one order of magnitude or more for long alkanes or large species such as benzene. In Section 5, we summarize our findings and make some final remarks.

2 Time-Dependent Renormalization Group Theory

Before specializing to the case of diffusion of ions or polarizable species at low densities in disordered zeolites, we first consider the more general problem of diffusion of any type of species in a disordered environment. In general, the disorder will slow down the diffusing species, and we would like to predict the magnitude of this effect and the characteristic time scale at which it occurs. Since we will be interested only in the ratio of the macroscopic diffusivity to the microscopic diffusivity, we can use a theory valid for long times and large distances. Field theory is just such a tool. Field theory also naturally allows us to

consider the effect of the disordered environment. Alternatively, field theory can be viewed as one particularly effective way to solve for the Green function of this diffusion problem. Interactions between the diffusing species will be negligible at low densities, even for ionic species.^{12,13} We, therefore, consider the single-species diffusion equation

$$\frac{\partial G_v(\mathbf{x}, t)}{\partial t} = D_0 \nabla^2 G_v(\mathbf{x}, t) + \beta D_0 \nabla \cdot [G_v(\mathbf{x}, t) \nabla v(\mathbf{x})] \quad (1)$$

Here v is the quenched random energy field caused by the disorder, G_v is the Green function of a single diffusing species in a given realization of the disorder, D_0 is the “bare,” short-time diffusivity, and $\beta = 1/(k_B T)$ is the inverse temperature. The mean-square displacement is given by $R_v^2(t) = \int d^d \mathbf{x} |\mathbf{x}|^2 G_v(\mathbf{x}, t)$. The mean-square displacement measured in an experiment is averaged over the statistics of the disorder: $R^2(t) = \langle R_v^2(t) \rangle = \int d^d \mathbf{x} |\mathbf{x}|^2 G(\mathbf{x}, t)$, where the Green function averaged over disorder is $G(\mathbf{x}, t) = \langle G_v(\mathbf{x}, t) \rangle$.

Because we are interested only in how the large-distance features of the random environment affect the diffusive motion, we can use a particularly simple, Gaussian form for the disordered energy field. Other forms turn out to be equivalent to this choice in a certain, technical sense. Since the force on a diffusing species is proportional to the gradient of the energy field, we can set the average value of the field to zero without loss of generality. And since we assume it is Gaussian, the only other quantity to specify is the energy-energy correlation function $\chi_{vv}(\mathbf{r}) = \langle v(\mathbf{0})v(\mathbf{r}) \rangle$.

The time-dependent field theory and model we use has been analyzed extensively in the context of reaction and diffusion processes in random media.^{14,15} Here we consider only the diffusion process. In this section, we derive a formula for the time-dependent self-diffusivity,

which is defined as

$$D(t) = \frac{R^2(t)}{2dt} \quad (2)$$

For the application to zeolites we will consider $d = 3$ dimensions, but here we develop the theory for a general spatial dimension.

The derivation of the field theory is somewhat technical,^{14,15} and so we provide a summary of the procedure here. A master equation that describes the motion of the diffusing species is first written. This master equation is equivalent to eq 1. The master equation is then rewritten in terms of creation and annihilation operators. The coherent state representation is then used to rewrite the master equation in terms of a field theory. Finally, the replica trick is used to integrate out the effects of the disorder. After these exact transformations, one arrives at the action $S = S_0 + S_I$, with

$$S_0 = \sum_{\alpha=1}^N \int d^d \mathbf{x} \int_0^\infty dt \bar{a}_\alpha(\mathbf{x}, t) [\partial_t - D_0 \nabla^2 + \delta(t)] a_\alpha(\mathbf{x}, t) \quad (3)$$

$$S_I = \frac{\beta^2 D_0^2}{2} \sum_{\alpha, \gamma=1}^N \int_0^\infty dt_1 dt_2 \int_{\mathbf{k}_1 \mathbf{k}_2 \mathbf{k}_3 \mathbf{k}_4} (2\pi)^d \delta(\mathbf{k}_1 + \mathbf{k}_2 + \mathbf{k}_3 + \mathbf{k}_4) \\ \hat{a}_\alpha(\mathbf{k}_1, t_1) \hat{a}_\alpha(\mathbf{k}_2, t_1) \hat{a}_\gamma(\mathbf{k}_3, t_2) \hat{a}_\gamma(\mathbf{k}_4, t_2) \\ \mathbf{k}_1 \cdot (\mathbf{k}_1 + \mathbf{k}_2) \mathbf{k}_3 \cdot (\mathbf{k}_1 + \mathbf{k}_2) \hat{\chi}_{vv}(|\mathbf{k}_1 + \mathbf{k}_2|) \quad (4)$$

The Fourier transform of a function is defined by $\hat{f}(\mathbf{k}) = \int d^d \mathbf{x} f(\mathbf{x}) \exp(i\mathbf{k} \cdot \mathbf{x})$, and the notation $\int_{\mathbf{k}}$ is a short hand for $\int d^d \mathbf{k} / (2\pi)^d$. The number of replicas is N , and the $N \rightarrow 0$ limit is implied. The action is used to calculate averages. The Green function, for example, is given by

$$G(\mathbf{x}, t) = \lim_{N \rightarrow 0} \frac{1}{N} \sum_{i=1}^N \langle a_i(\mathbf{x}, t) \bar{a}_i(\mathbf{0}, 0) \rangle \quad (5)$$

where the average is with respect to the weight $\exp(-S)$. The free theory term S_0 represents simple diffusion. The interaction term S_I comes from averaging the diffusion process over the random energy field, which is again assumed to be Gaussian, with zero mean and correlation function $\hat{\chi}_{vv}$. The form of $\hat{\chi}_{vv}$ is left general throughout the calculation.

Using field theoretic renormalization group theory¹⁶ we let $\bar{a} \rightarrow Z_a^{\frac{1}{2}}\bar{a}$, $a \rightarrow Z_a^{\frac{1}{2}}a$, $D \rightarrow Z_a^{-1}Z_D D$, and $\beta^2 \rightarrow \beta^2 Z_D^{-2}Z_I$. Note that the dimensions of $\beta^2\hat{\chi}_{vv}$ are the same as that of k^{-d} , where k has the dimensions of wave number. We have chosen β as dimensionless in this renormalization scheme. The Z factors will be determined by a subtraction scheme. Following a one-loop calculation of the renormalized vertex functions in the long-time limit, we find

$$\begin{aligned} Z_a &= 1 \\ Z_D &= 1 - \frac{\beta^2 K_d}{d} \int_{\mu}^{\Lambda} dk k^{d-1} \hat{\chi}_{vv}(k) \\ Z_I &= 1 - \frac{2\beta^2 K_d}{d} \int_{\mu}^{\Lambda} dk k^{d-1} \hat{\chi}_{vv}(k) \end{aligned} \quad (6)$$

where $K_d = S_d/(2\pi)^d$, $S_d = 2\pi^{d/2}/[\Gamma(d/2)]$ is the surface area in d dimensions, Λ is a cut-off, and $\mu = \Lambda/e^l$ with l the flow parameter. No contribution renormalizes the time derivative or delta function term in S_0 . The associated renormalization-group functions are defined by

$$\gamma_i = \mu \left. \frac{\partial \ln Z_i}{\partial \mu} \right|_0, \quad i = a, D, I \quad (7)$$

where the subscript 0 on the derivative indicates fixed bare variables. We find

$$\begin{aligned}
\gamma_a &= 0 \\
\gamma_D &= \beta^2 K_d \mu^d \hat{\chi}_{vv}(\mu)/d \\
\gamma_I &= 2\beta^2 K_d \mu^d \hat{\chi}_{vv}(\mu)/d
\end{aligned} \tag{8}$$

and

$$\beta_I = \mu \left. \frac{\partial \beta^2}{\partial \mu} \right|_0 = (\gamma_I - 2\gamma_D)\beta^2 = 0 \tag{9}$$

The dynamical exponent is given by

$$z = 2 - \gamma_a + \gamma_D = 2 + \beta^2 K_d \mu^d \hat{\chi}_{vv}(\mu)/d \tag{10}$$

The renormalized time flows according to

$$t(l^*) = t \exp \left[- \int_0^{l^*} z(l) dl \right] = t_0 \tag{11}$$

The matching time, t_0 , is usually on the order of $1/(\Lambda^2 D_0)$, which is within the range of validity of both renormalization group scaling and mean field theory. The Callan-Symanzik equation then reads

$$\left(\mu \frac{\partial}{\partial \mu} - \gamma_D \right) D = 0 \tag{12}$$

Solving this differential equation, we find

$$D(l^*) = D(0) \exp \left[-\frac{\beta^2 K_d}{d} \int_0^{l^*} dl \left(\frac{\Lambda}{e^l} \right)^d \hat{\chi}_{vv} \left(\frac{\Lambda}{e^l} \right) \right] \quad (13)$$

An explicit form for $D(t)$ follows from eq 13 after relating the flow parameter l^* to time by eqs 10 and 11

$$\begin{aligned} D(t) &= D_0 \exp \left[-\frac{\beta^2 K_d}{d} \int_0^{l^*(t)} dl \left(\frac{\Lambda}{e^l} \right)^d \hat{\chi}_{vv} \left(\frac{\Lambda}{e^l} \right) \right] \\ &= D_0 \exp \left[-\frac{\beta^2 K_d}{d} \int_{\Lambda/e^{l^*}}^{\Lambda} dk k^{d-1} \hat{\chi}_{vv}(k) \right] \end{aligned} \quad (14)$$

In the limit of $t \rightarrow \infty$, which implies $l^* \rightarrow \infty$, the above equation yields

$$D_\infty = D_0 \exp[-\beta^2 \chi_{vv}(0)/d] \quad (15)$$

which is in agreement with the long-time renormalization group result found in Refs 10 and 17. Finally, eq 11 can be rewritten as

$$t = t_0 e^{2l^*} D_0/D(t) \quad (16)$$

The renormalization result depends on the matching time t_0 appearing in eq 11. We determine t_0 by equating perturbation theory to the renormalization group result for weak disorder, or equivalently, $\beta \rightarrow 0$. The mean square displacement is given by $R^2(t) = 2dDt$,

so the diffusivity is related to the Green function by

$$D(t) = \frac{\int d^d \mathbf{x} x^2 G(\mathbf{x}, t)}{2dt} = -\frac{\nabla_{\mathbf{k}}^2 \hat{G}(\mathbf{k}, t)|_{\mathbf{k}=0}}{2dt} \quad (17)$$

For weak disorder, perturbation theory gives

$$D(t) = D_0 - \frac{\beta^2 K_d}{dt} \int_0^\Lambda dk k^{d-3} \hat{\chi}_{vv}(k) (-3 + x + 3e^{-x} + 2xe^{-x}) + O(\beta^4, t^3) \quad (18)$$

where $x \equiv D_0 k^2 t$. In the limit $\beta \rightarrow 0$ we match perturbation theory and the renormalization group theory at a characteristic time, t_c :

$$D(t_c) = (D_0 + D_\infty)/2 = D_0 - \frac{D_0 \beta^2 \chi_{vv}(0)}{2d} + O(\beta^4) \quad (19)$$

We find t_c by equating eqs 18 and 19 to $O(\beta^2)$:

$$\chi_{vv}(0) = \frac{2K_d}{D_0 t_c} \int_0^\Lambda dk k^{d-3} \hat{\chi}_{vv}(k) (-3 + x_c + 3e^{-x_c} + 2x_c e^{-x_c}) \quad (20)$$

where $x_c = D_0 k^2 t_c$. Note that eq 20 shows that t_c is a function of Λ , D_0 , and the form of $\hat{\chi}_{vv}$, but not the strength of the disorder. We similarly find l_c by equating eqs 14 and 19 to $O(\beta^2)$:

$$\chi_{vv}(0) = 2K_d \int_0^{l_c} dl \left(\frac{\Lambda}{e^l}\right)^d \hat{\chi}_{vv}\left(\frac{\Lambda}{e^l}\right) \quad (21)$$

We finally obtain t_0 at small β^2 from the relation, $t_0 = t_c e^{-2l_c}$. We assume that t_0 is only weakly dependent on the strength of the disorder and use the same t_0 for all values of β^2 .

3 Monte Carlo Simulation Results

Before we apply the time-dependent theory to diffusion in disordered microporous materials, we first test it against computer simulations. We do this by generating numerical solutions to eq 1, averaging them over the statistics of the disorder, and then comparing the results to eq 14. The computer simulations are done on a lattice in two dimensions and follow closely the strategy of Ref 18. Using eqs (3-10) from Ref 18, we create a Gaussian random energy field, prescribed by $\hat{v}(k)$, on a lattice. We determine the energy field in real space by fast Fourier transform. To obtain reasonable statistics for the diffusivity, we follow the motion of 10000 independent particles on a lattice of size L . Periodic boundary conditions are enforced. We use lattices of size $L = 512, 1024, \text{ and } 2048$ in order to identify and avoid finite size effects. The initial particle positions are chosen at random. Finally, $D(t)$ is measured by averaging $R^2(t)$ as a function of t over a moving window of 200 Monte Carlo steps and evaluating the slope. To test the robustness of the theory, we examined three forms of $\hat{\chi}_{vv}$: $\hat{\chi}_{vv} = \gamma \exp[-k^2/(2k_c^2)]$, $\hat{\chi}_{vv} = \gamma \exp(-|k|/k_c)$, and $\hat{\chi}_{vv} = \gamma k_c^4/(k^2 + k_c^2)^2$.

The simulation results with $L = 2048$ and $k_c = 0.1$ are shown in Figure 1-3 for each form of $\hat{\chi}_{vv}$. Significantly, the infinite time result for the diffusivity, eq 15, appears exact to within the statistics of our simulation. More importantly for the present purpose, there is a good agreement between the renormalization group result, eq 14, and the simulation data over the entire time range. Indeed, t_0 appears to be only weakly dependent on the strength of disorder. Recall that t_0 was determined at weak disorder, and we assumed it to be constant at strong disorder. The observed constancy of t_0 validates our matching procedure.

Interestingly, two types of finite size effects can occur in these simulations. First, the

lattice must be large enough to capture the length scale at which the disorder begins to slow down the diffusing species. If the lattice is not large enough, the diffusivity will reach the proper asymptotic, long-time value. Second, the lattice must be fine enough so as to capture all of the features inherent in the chosen $\chi_{vv}(\mathbf{x})$. If the characteristic length of $\chi_{vv}(\mathbf{x})$ is finer than the lattice spacing, then some of the effects of the random energy field will be lost. Since the diffusion constant decreases with increasing disorder, a lattice that is not fine enough and, therefore, neglects some of the effects of the disorder, will predict a diffusivity that is too large. We, indeed, observe this effect for simulations with $k_c = 1.0$. In this case, the characteristic size $r_c = 2\pi/k_c$ is approaching the lattice spacing of unity that we use.

Note that we observe a peak of $D(t)/D_0$ in the simulations for small $D_0 k_c^2 t$. This peak is more evident for small values of k_c . In Figure 4 we plot the simulation results together with the renormalization group and short-time perturbation theory results for $k_c = 0.02$. It is clear that perturbation theory describes the short-time peak well. This is to be expected since the perturbation result is accurate to $O(t^2)$ for all values of β^2 . In contrast, the renormalization group approach fails to predict this interesting short-time behavior, since the renormalization procedure is carried out in the asymptotic, long-time limit. This peak in the diffusivity is due to the rapid relaxation of the particles away from the initial, non-equilibrium distribution. Consequently, this peak would not be expected to be observed in equilibrium techniques such as NMR, PFG NMR, or QENS.

4 Time-Dependent Diffusion in Zeolites

Within a zeolite crystal there is a random potential field, mainly due to the random electrostatic potential created by the charged framework Al^- and non-framework cation sites. The lattice defects, cations, and associated aluminum atoms create strong disorder, increase the hopping activation energy, inhibit the mobility of sorbates, and slow down the diffusion process. We list the ionic self-diffusivities measured in same-type of zeolites with different aluminum loadings in Table 1. To reduce the effects of ionic hydration, data taken for methanol or ethanol solvents are exhibited. As can be seen, Table 1 confirms a reduction diffusivity caused by aluminum-induced disorder. That is, at higher aluminum loadings the activation energy increases and the diffusivity decreases.

We assume that the spatial arrangement of the charges in zeolites is fixed during formation conditions, i.e. that the disorder is quenched.¹⁹ The Debye-Hückel theory²⁰ for the density-density correlation function of the charged impurities then gives

$$\hat{\chi}_{\rho\rho}(k) = \frac{\gamma k^2}{k^2 + \kappa^2} \quad (22)$$

with $\gamma = |e^-|^2(\rho_+ + \rho_-)$, and κ is an inverse characteristic length of the charged disorder, defined by $\kappa^2 = \beta_{\text{F}}|e^-|^2(\rho_+ + \rho_-)/\epsilon_{\text{F}}$. Here e^- is the electron charge, ρ_+ and ρ_- are the positive and negative charge number densities, respectively, ϵ_{F} is the dielectric constant under formation conditions, and $\beta_{\text{F}} = 1/(k_{\text{B}}T_{\text{F}})$ with T_{F} the formation temperature. Under typical aqueous synthesis conditions of $\text{pH} = 12$ and $T_{\text{F}} = 398 \text{ K}$, the dielectric constant ϵ_{F} is approximately $\epsilon_{\text{F}} = 50\epsilon_0$.²¹ The correlation function of the electrostatic potential due to

the charged impurities is:

$$\hat{\chi}_{\phi\phi}(k) = \frac{\hat{\chi}_{\rho\rho}(k)}{\epsilon^2 k^4} \quad (23)$$

where now the dielectric constant should be the value in the zeolitic solid, i.e. $\epsilon = 4.2\epsilon_0$.²¹

We first consider the diffusion of an ion of charge q in such a zeolite. The energy-energy correlation function due to the charged disorder is

$$\hat{\chi}_{vv}^{\text{ion}}(k) = q^2 \hat{\chi}_{\phi\phi}(k) \quad (24)$$

We consider diffusion of a singly charged species, $q = |e^-|$, at room temperature. We take zeolite NaY with $\rho_{\text{T}} = 1.27 \times 10^{28} \text{ m}^{-3}$ and $\rho_{\text{Al}} = 0.3 \rho_{\text{T}}$ as our example, where ρ_{T} is the density of T (=Si or Al) atoms in the zeolite. We are interested in the magnitude of the time-dependent diffusivity as well as the characteristic time, t_c . It appears at first sight that our theory requires no cutoff. Directly solving eq 15 and 20, we find $D_{\infty}/D_0 = e^{-634}$, and $D_0 \kappa^2 t_c = 8.8$. The term $\beta^2 \chi(0)/d$ in the exponential of eq 15 looks like an activation energy introduced by disorder, but the numerical result, $\beta E = 634$, is significantly larger than that measured in experiments.²²

It is, however, clear that Debye-Hückel theory is not quite right for short distances or large wave vectors. In particular, the characteristic length of the charged disorder, $2\pi/\kappa$, is typically on the order of several Ångströms. Motion on the Ångströms length scale is measured in microscopic experiments such as NMR and is well described by Newton's equation, e.g. by molecular dynamics simulations. Statistical field theory is applicable only for behavior at much longer time or length scales, and so D_0 is an input parameter, determined

from a simulation or a short-time experiment. Since this D_0 already captures short time and distance properties, a cutoff is required to exclude these effects. This cutoff will be a function of κ . Given the measured diffusivity and the experimental time scale, t_{exp} , however, the cutoff can be calculated by

$$\begin{aligned}\Lambda_{\text{exp}} &= 2\pi/r_{\text{exp}} \\ r_{\text{exp}}^2 &= 2D_0t_{\text{exp}}\end{aligned}\tag{25}$$

Physically this means that we should use field theory only to consider fluctuations with wavelengths larger than r_{exp} .

Many factors, such as charge neutrality, Loewenstein's rule, strong cation hydration, ion-sieving effects, and the existence of several different energetically favorable cation sites, all complicate the cationic diffusion process and make ion diffusion data hard to organize.¹ In Table 2, we illustrate the effect of disorder for a few typical diffusivities. Since the available techniques for measuring cation diffusion in zeolites, such as tracer exchange or counter diffusion exchange, are at the time scale of minutes, we use $t_{\text{exp}} = 100$ s. From Table 2, we see that a smaller D_0 leads to a larger cutoff and a larger correction to the diffusivity. For example, if $D_0 = 1 \times 10^{-10} \text{ m}^2\text{s}^{-1}$ we see $D_\infty/D_0 = 1$ and no correction, while with $D_0 = 1 \times 10^{-17} \text{ m}^2\text{s}^{-1}$ we see a significant correction of $D_\infty/D_0 = 0.002$. For all these cases, the cutoff Λ_{exp} obtained is much smaller than κ , and so the field-theoretic approach is appropriate. By assuming $\Lambda \ll \kappa$, we can further simplify the energy-energy correlation function as

$$\hat{\chi}_{vv}(k) = \frac{\eta}{k^2}; \text{ with } \eta = \frac{q^2\epsilon_{\text{F}}}{\beta_{\text{F}}\epsilon^2}\tag{26}$$

From this form of $\hat{\chi}$, we find

$$D_\infty = D_0 \exp[-\beta^2 K_d \eta \Lambda_{\text{exp}}/d] \quad (27)$$

Solving for t_c from eq 20, we find

$$\Lambda_{\text{exp}}^2 D_0 t_c = 37.3 \quad (28)$$

and from eq 21, we find

$$t_0 = t_c/4 \quad (29)$$

From eq 25 we see immediately that $t_c \propto t_{\text{exp}}$, which explains why we would have the same value of t_c for the different diffusivities in Table 2. When the diffusivity is dramatically reduced, the characteristic time is better defined as the time at which the measured diffusivity is very close to D_∞ , i.e. $D(t_{90\%}) = 1.1D_\infty$. We have calculated $t_{90\%}$ numerically from eqs 14 and 16 and list the values in Table 2. As expected, $t_{90\%}$ increases with decreasing D_∞/D_0 . Interestingly, we find the mean-square distance that ions diffuse within this time period is constant:

$$\Delta x_{90\%} = [R^2(t_{90\%})/3]^{1/2} = \frac{\beta^2 \eta}{3\pi \ln(1.1)} \left[\frac{t_0}{t_{\text{exp}}} \right]^{1/2} \quad (30)$$

We now turn to consider the case of diffusion of polarizable species in zeolites. The energy of a polarizable species in an electric field is given by $v(\mathbf{x}) = -\frac{1}{2}\alpha|\nabla\phi(\mathbf{x})|^2$, where α is the molecular polarizability, and ϕ is the electric potential. Using the Gaussian approximation for ϕ , we find the energy-energy correlation function of polarizable species to

be

$$\hat{\chi}_{vv}^{\text{polarizable}}(\mathbf{k}) = \frac{1}{2}\alpha^2 \int_{\mathbf{p}} [(\mathbf{p} - \mathbf{k}) \cdot \mathbf{p}]^2 \hat{\chi}_{\phi\phi}(\mathbf{p} - \mathbf{k}) \hat{\chi}_{\phi\phi}(\mathbf{p}) \quad (31)$$

A cut-off is necessary to ensure the convergence of this integral. As before, this cutoff must be smaller than κ if the field theory is to be applicable. Furthermore, the length scale should also be on the order of or larger than a molecular size and roughly equal to the displacement of molecules on the microscopic experimental time scale. We simply set $\Lambda = 2\pi/(5\text{\AA})$.

We list results of the calculation for the four species H_2 , CH_4 , C_4H_{10} , and C_6H_6 in Table 2. For H_2 , the transport and self-diffusion coefficients were measured simultaneously in Ref 5 by QENS. No discrepancy was found, and the diffusivities given by the two methods are in good agreement with each other, $D_0 = 3 \times 10^{-9} \text{m}^2\text{s}^{-1}$ at $T = 100 \text{K}$ in NaX. Methane serves as another example where no discrepancies have been reported. The diffusivity of methane in NaX measured by QENS is $3.2 \times 10^{-9} \text{m}^2\text{s}^{-1}$.²³ Our calculations support the lack of discrepancy in these cases. Although the characteristic time scales lie just within the range of QENS experiments, the calculated D_∞/D_0 for H_2 and CH_4 is 0.72 and 0.39 respectively. Such a ratio would be difficult to observe, given the small characteristic times.

Numerous experiments have reported that there are two orders of magnitude of discrepancy between the microscopic and macroscopic diffusion of benzene in NaX or NaY.⁶ Computer simulations by Auerbach *et al.* of benzene diffusion in Na-X or NaY suggest that the longer time scale PFG-NMR technique measures intercage diffusion, while the short time scale NMR spin-lattice relaxation technique measures intracage diffusion.^{8,11,24} These simulations also suggest that the cage-to-cage length, 11\AA , is a reasonable approximation for the effective hopping length. Our cutoff should be smaller than this value to capture the effects

of disorder on this length scale. We use the microscopic $D_0 = 1.9 \times 10^{-10} \text{ m}^2\text{s}^{-1}$ measured by the QENS method.²⁵ With our chosen cutoff, our theory predicts $t_{90\%} = 4.4 \times 10^{-8} \text{ s}$ and $D_\infty/D_0 = 0.08$. The large characteristic time is primarily due to the smaller diffusivity for benzene compared to hydrogen or methane. For this species, the greater discrepancy in diffusivity is primarily due to the greater polarizability of benzene compared to hydrogen or methane. For this species, we may expect to see the time-dependence of the diffusivity in QENS experiments, or we may expect to see discrepancies between microscopic and macroscopic measurements.¹ Consistent with the idea that increased disorder slows down the diffusion species, benzene diffusivities observed in simulations also decrease with increased aluminum loading.¹¹ For butane, the calculated D_∞/D_0 is small. Since the characteristic time $t_{90\%}$ lies within the range of QENS, we may be able to observe a discrepancy in this case as well.

Instead of imposing a length-scale cutoff for diffusion of the polarizable species, we may impose a time-scale cutoff, as we did in Table 2. We choose $t_{\text{exp}} = 10^{-9} \text{ s}$, since this is at the lower end of the time scale accessible to QENS and near the upper end of the time scale accessible to molecular dynamics. We use eq 25 to derive the value of Λ_{exp} to use in our calculations. The results are listed in Table 3. With this type of cutoff, we find a discrepancy between microscopic and macroscopic measurements only for benzene. Comparison of the results in Tables 2 and 3 shows that differences between microscopic and macroscopic measurements depend sensitively on the details of the time or length scale resolved by the microscopic experimental technique. Experimental diffusivities may be less sensitive to the cutoff procedure than these tables would suggest, since the Gaussian approximation that we have used has led to an over-sensitivity to short-distance features in the case of polarizable

species.

On the other hand, diffusion data for many species in zeolite A are in satisfactory agreement.² This seems at odds with our theory, since in zeolite A, the Si:Al ratio is as high as unity. However, a closer examination of the structure of zeolite A reveals a perfect crystal structure. The aluminum ions obey Loewenstein's rule and are arranged in a highly symmetrical way, such that each unit cell consists of 96 AlO_4 and 96 SiO_4 tetrahedra with each apical oxygen atom shared between one aluminum atom and one silicon atom. Zeolite A is not disordered, and so the movement of molecules within each unit cell rapidly reaches diffusive behavior. We, therefore, do not expect to observe any long time corrections to diffusivities in zeolite A. Although the Si:Al ratio is close to unity in zeolite X as well, the unit cell is significantly larger and the electrostatic potential is substantially disordered compared to zeolite A, as judged by the presence of the strong electric field gradients that make X-type zeolites suitable for selective separation of air.⁹ It is this disorder that can lead to a time-dependent diffusivity.

We can summarize our results by noting that the characteristic time for the slowing down of the diffusing species due to disorder is given by $t_c = \xi^2/(2D_0)$, where ξ is a characteristic length associated with the disorder. Smaller values of D_0 , therefore, lead to larger characteristic times and a greater chance that a discrepancy between microscopic and macroscopic measurements will occur. We have considered only two contributions to the force on a diffusing species, the Coulombic force on ions and the induced-dipole force on polarizable species. Other interactions between the diffusing species and the zeolite framework and non-framework atoms, such as ion-dipole, ion-quadrupole, Lennard-Jones, and so on, also contribute to the random energy fields. These additional terms would also slow down the dif-

fusing species, although the characteristic times of most of these interactions are too short to cause an observable discrepancy between microscopic and macroscopic measurements. Our calculations for diffusion of ions should be fairly robust, since in this case there is especially good reason to believe that the disorder is well-approximated by a Gaussian.¹⁰ For polarizable species, our calculated corrections to the short-time diffusivity are sensitive to the numerical value of the cutoff. Equivalently, the theory is sensitive to the assumptions about the behavior of the dielectric constant at short distances. We have also assumed that the time scales associated with configurational arrangement of the diffusing, polarizable species are much shorter than the characteristic diffusion time induced by the disorder. Our predictions for the ionic case, therefore, are more quantitatively reliable than those for the polarizable case. Regardless of the details, that disorder induces a time-dependent diffusivity, as in eq refeq2, for an ionic or polarizable species is a general result.

Disorder on longer mesoscopic length scales can also occur in zeolites in the form of faulting or growth-induced domain-mismatch. The length scales associated with such domains can be on the order of $\xi = 10$ nm in the ZSM-5²⁶ and Linde Type L²⁷ zeolites. It would be interesting to see if a reduction in the diffusivity occurring at $t_c = \xi^2/(2D)$ is observable experimentally for these materials.

5 Conclusion

We have derived a time-dependent theory of diffusivity in disordered microporous media. As judged by computer simulations, the theory is reasonably accurate for Gaussian-type disorder over the entire time range. Applying the theory to zeolites, we offer disorder as one

possible mechanism for the existence of a discrepancy between microscopic and macroscopic measurements of diffusion in zeolites. For diffusion of ionic species, we predict that a discrepancy almost certainly exists. For polarizable species such as H_2 and CH_4 we predict no observable discrepancy, and none has been observed experimentally. Our study of benzene and n-butane suggests that disorder may cause a discrepancy for these molecules. The characteristic time and magnitude of the discrepancy are consistent with microscopic and macroscopic experimental observations. We explain the lack of a discrepancy for zeolite A as resulting from a lack of disorder in this highly-symmetric, perfectly-crystalline material.

Our theory can only predict the ratio $D(t)/D_0$. Determination of the short-time diffusivity, D_0 , is best done by a molecular dynamics simulation or a microscopic experiment. In this respect, molecular dynamics simulation is a particularly useful, complementary tool to the field theory presented here. Diffusivities derived by molecular dynamics are often comparable with the NMR, PFG NMR, and QENS measurements.²⁸ Moreover, simulation provides molecular details beyond the scope of an experiment or a field theory. Such simulations should, for example, allow one to construct a more exact form of $\hat{\chi}_{vv}(k)$ to be used in our theory.

Acknowledgments

We thank Jeong-Man Park for useful discussions. This research was supported by Chevron Research and Technology Company and by the National Science Foundation through grant number CTS-9702403.

References

- [1] Kärger, J.; Ruthven, D. M. *Diffusion in Zeolites and other Microporous Solids*; John Wiley & Sons, Inc: New York, 1991 especially Chapter 15.
- [2] Eic, M.; Ruthven, D. M. *Zeolites* **1988**, *8*, 472-479.
- [3] Sun, M. S.; Talu, O.; Shah, D. B. *AIChE J.* **1996**, *42*, 3001-3007.
- [4] Kärger, J.; Pfeifer, H.; Rauscher, M.; Walter, A. *J.C.S. Faraday I* **1980**, *76*, 717-737.
- [5] Jobic, H.; Kärger, J.; Bée, M. *Phys. Rev. Lett.* **1999**, *82*, 4260-4263.
- [6] Ref. 1, p. 515.
- [7] Runnebaum, R. C.; Maginn, E. J. *J. Phys. Chem. B* **1997**, *101*, 6394-6408.
- [8] Auerbach, S. M.; Henson, N. J.; Cheetham, A. K.; Metiu, H. I. *J. Phys. Chem.* **1995**, *99*, 10600-10608.
- [9] Newsam, J. M. Zeolites. In *Solid State Chemistry: Compounds*; Cheetham, A. K.; Day, P., Eds.; Oxford University Press: Oxford, 1992.
- [10] Deem, M. W.; Chandler, D. *J. Stat. Phys.* **1994**, *76*, 911-927.
- [11] Auerbach, S. M.; Metiu, H. I. *J. Chem. Phys.* **1997**, *106*, 2893-2905.
- [12] Park, J.-M.; Deem, M. W. *Phys. Rev. E* **1998**, *58*, 1487-1493.
- [13] Deem, M. W. *Phys. Rev. Lett.* **1999**, *83*, 1694.
- [14] Deem, M. W.; Park, J.-M. *Phys. Rev. E* **1998**, *57*, 2681-2685.

- [15] Park, J.-M.; Deem, M. W. *Phys. Rev. E* **1998**, *57*, 3618-3621.
- [16] Zinn-Justin, J. *Quantum Field Theory and Critical Phenomena*; Clarendon Press: Oxford, 3rd ed.; 1996 Chapter 11.
- [17] Dean, D. S.; Drumond, I. T.; Horgan, R. R. *J. Phys. A: Math. Gen.* **1994**, *27*, 5135–5144 Figure 8.
- [18] Pham, V.; Deem, M. W. *J. Phys. A: Math. Gen.* **1998**, *31*, 7235-7247.
- [19] Ma, S. K. *Modern Theory of Critical Phenomena*; volume 46 of *Fronteiers in Physics* The Benjamin/Cummings Publishing Company, Inc: London, 1976 Chapter X.
- [20] Netz, R. R.; Orland, H. *Europhys. Lett.* **1999**, *45*, 726-732.
- [21] Lide, D. R., Ed.; *CRC handbook of Chemistry and Physics*; CRC Press: New York, 80th ed.; 1999.
- [22] Barrer, R. M. Zeolite Exchangers-Some Equilibrium and Kinetic Aspects. In *Proceedings of the fifth international conference on zeolites*; Rees, L. V. C., Ed.; Heyden: London, 1980 Table 3.
- [23] Jobic, H.; Bée, M.; Kearley, G. J. *J. Phys. Chem.* **1994**, *98*, 4660-4665.
- [24] Auerbach, S. M.; Bull, L. M.; Henson, N. J.; Metiu, H. I.; Cheetham, A. K. *J. Phys. Chem.* **1996**, *100*, 5923-5930.
- [25] Jobic, H.; Bée, M.; Kärger, J.; Pfeifer, H.; Caro, J. *J. Chem. Soc., Chem. Comm.* **1990**, 341–342.

- [26] de Moor, P. E. A.; Beelen, T. P. M.; Komanschek, B. U.; Beck, L.; Wagner, P.; Davis, M.; van Santen, R. *Chem. Eur. J.* **1999**, *5*, 2083-2088 Figure 3.
- [27] Nikolakis, V.; Vlachos, D. G.; Tsapatsis, M. *J. Chem. Phys.* **1999**, *111*, 2143–2150.
- [28] Clark, L. A.; Ye, G. T.; Gupta, A.; Hall, L. L.; Snurr, R. Q. *J. Chem. Phys.* **1999**, *111*, 1209-1222.

Table 1: Measurements of self diffusivities and activation energies in zeolite Y with different Al content.²²

| Zeolite | Si:Al | $\rho_{\text{Al}}/\rho_{\text{T}}^a$ | Solvent | E (kJ/mol) | D (m ² s ⁻¹) |
|---------|--------|--------------------------------------|----------|------------|-------------------------------------|
| Sr-Y | 139:53 | 0.276 | Methanol | 91.6 | 5.2×10^{-22} |
| Sr-Y | 125:67 | 0.349 | Methanol | 118 | 1.4×10^{-25} |
| Ba-Y | 139:53 | 0.276 | Methanol | 67.8 | 3.3×10^{-20} |
| Ba-Y | 125:67 | 0.349 | Methanol | 84.1 | 1.5×10^{-21} |
| Ba-Y | 139:53 | 0.276 | Ethanol | 91.6 | 3.3×10^{-24} |
| Ba-Y | 125:67 | 0.349 | Ethanol | 120 | 3.1×10^{-25} |

^a ρ_{T} is the density of framework T (=Si or Al) atoms.

Table 2: Ionic diffusivities in NaY with $\rho_{\text{Al}} = 0.3 \rho_{\text{T}}$ and $T = 298$ K.

| D_0 (m ² s ⁻¹) | t_{exp} (s) | Λ_{exp} (m ⁻¹) | D_{∞}/D_0 | $t_{90\%}$ (s) | $\Delta x_{90\%}$ (m) |
|---|----------------------|---|------------------|----------------------|-----------------------|
| 1×10^{-10} | 100 | 4.4×10^4 | 1 | - | - |
| 1×10^{-14} | 100 | 4.4×10^6 | 0.82 | 230 | 2.03×10^{-6} |
| 1×10^{-15} | 100 | 1.4×10^7 | 0.53 | 3.5×10^3 | 2.03×10^{-6} |
| 1×10^{-16} | 100 | 4.4×10^7 | 0.14 | 1.4×10^5 | 2.03×10^{-6} |
| 1×10^{-17} | 100 | 1.4×10^8 | 0.002 | 1.0×10^8 | 2.03×10^{-6} |
| 1×10^{-18} | 100 | 4.4×10^8 | e^{-20} | 8.6×10^{14} | 2.03×10^{-6} |

Table 3:

Characteristic time, length, and D_{∞}/D_0 for polarizable species with $\Lambda = 2\pi/(5\text{\AA})$.^a

| Species | Zeolite | $\rho_{\text{Al}}/\rho_{\text{T}}$ | T(K) | D_0 (m ² s ⁻¹) | Ref | $\alpha/(4\pi\epsilon_0)$ (m ³) ²¹ | D_{∞}/D_0 | $t_{90\%}$ (s) | $\Delta x_{90\%}$ (Å) |
|--------------------------------|---------|------------------------------------|------|---|-----|---|------------------|-----------------------|-----------------------|
| H ₂ | NaX | 0.5 | 100 | 3×10^{-9} | 5 | 0.8×10^{-30} | 0.72 | 7.1×10^{-11} | 5.8 |
| CH ₄ | NaY | 0.3 | 150 | 3.2×10^{-9} | 23 | 2.6×10^{-30} | 0.39 | 3.0×10^{-10} | 9.1 |
| C ₄ H ₁₀ | NaX | 0.5 | 298 | 2.5×10^{-9} | 6 | 8.2×10^{-30} | 0.02 | 2.0×10^{-8} | 15 |
| C ₆ H ₆ | NaX | 0.5 | 458 | 1.9×10^{-10} | 25 | 10×10^{-30} | 0.08 | 4.5×10^{-8} | 13 |

^aIf a short-distance dielectric constant of $\epsilon = 2.0\epsilon_0$ were used, a cutoff of $\Lambda = 2\pi/(9.5\text{\AA})$ would lead to similar values of D_{∞}/D_0 and characteristic times increased by roughly a factor of three.

Table 4:

Characteristic time, length, and D_{∞}/D_0 for polarizable species with $t_{\text{exp}} = 10^{-9}$ s.^a

| Species | Zeolite | $\rho_{\text{Al}}/\rho_{\text{T}}$ | T(K) | D_0 (m ² s ⁻¹) | Ref | $\alpha/(4\pi\epsilon_0)$ (m ³) ²¹ | D_{∞}/D_0 | $t_{90\%}$ (s) | $\Delta x_{90\%}$ (Å) |
|--------------------------------|---------|------------------------------------|------|---|-----|---|------------------|----------------------|-----------------------|
| H ₂ | NaX | 0.5 | 100 | 3×10^{-9} | 5 | 0.8×10^{-30} | 1 | - | - |
| CH ₄ | NaY | 0.3 | 150 | 3.2×10^{-9} | 23 | 2.6×10^{-30} | 1 | - | - |
| C ₄ H ₁₀ | NaX | 0.5 | 298 | 2.5×10^{-9} | 6 | 8.2×10^{-30} | 0.999 | - | - |
| C ₆ H ₆ | NaX | 0.5 | 458 | 1.9×10^{-10} | 25 | 10×10^{-30} | 0.37 | 7.5×10^{-9} | 11 |

^aIf a short-distance dielectric constant of $\epsilon = 2.0\epsilon_0$ were used, a $t_{\text{exp}} = 3.5 \times 10^{-9}$ s would lead to similar value of D_{∞}/D_0 and a characteristic time increased to 1.9×10^{-8} s for benzene

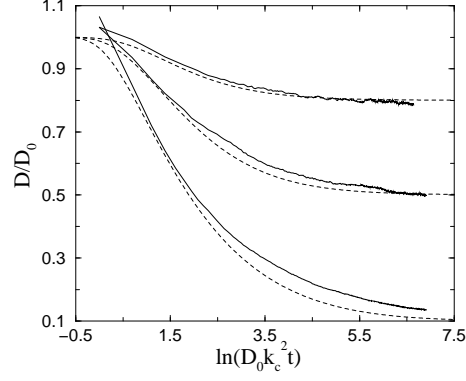


Figure 1: Comparison of the theoretical results (dashed) with simulation data (solid) for $\hat{\chi}_{vv}(k) = \gamma \exp[-k^2/(2k_c^2)]$, with $k_c = 0.1$. Three different values of γ were used corresponding to $D_\infty/D_0 = 0.8, 0.5$, and 0.1 , as predicted by eq 15.

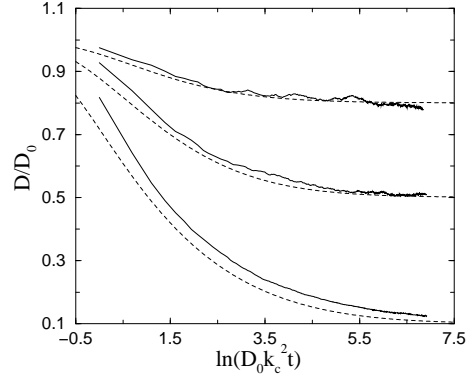


Figure 2: Comparison of the theoretical results (dashed) with simulation data (solid) for $\hat{\chi}_{vv}(k) = \gamma \exp(-|k|/k_c)$, with $k_c = 0.1$. Three different values of γ were used corresponding to $D_\infty/D_0 = 0.8, 0.5$, and 0.1 , as predicted by eq 15.

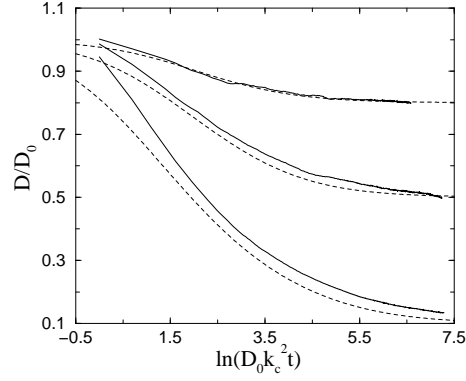


Figure 3: Comparison of the theoretical results (dashed) with simulation data (solid) for $\hat{\chi}_{vv}(k) = \gamma k_c^4 / (k^2 + k_c^2)^2$, with $k_c = 0.1$. Three different values of γ were used corresponding to $D_\infty/D_0 = 0.8, 0.5$, and 0.1 , as predicted by eq 15.

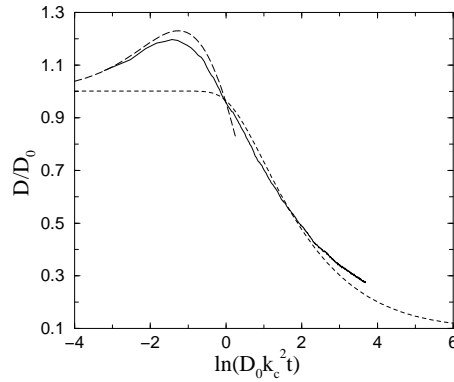


Figure 4: Comparison of the renormalization group (dashed) results with simulation data (solid) and short-time perturbation theory (long-dashed) for $\hat{\chi}_{vv}(k) = \gamma \exp[-k^2/(2k_c^2)]$, with $k_c = 0.02$ and $D_\infty/D_0 = 0.1$.